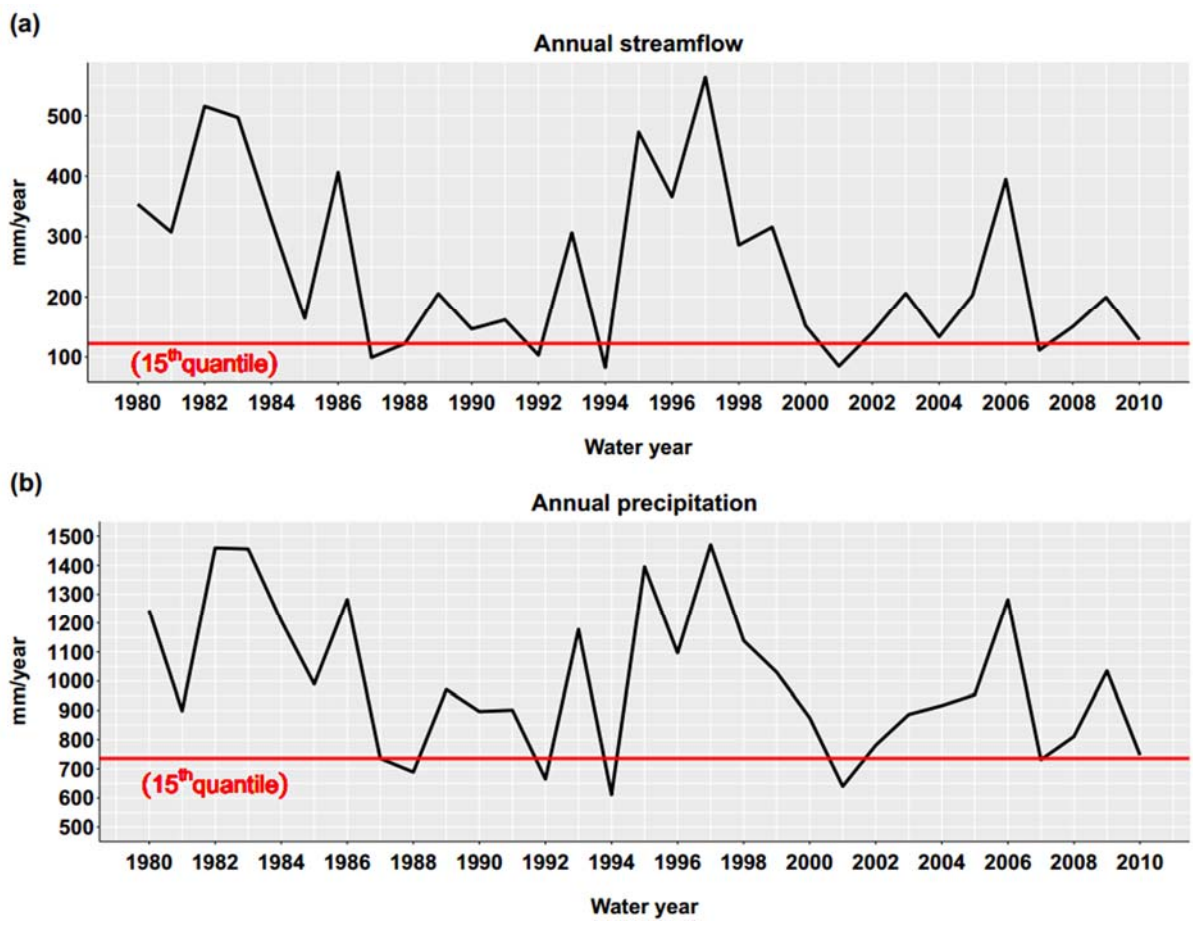


1 Supplement of
2 **How does water yield respond to mountain pine beetle infestation in a**
3 **semiarid forest?**

4 Jianning Ren et al.

5 *Corresponding to: Jennifer Adam (jcadam@wsu.edu)*

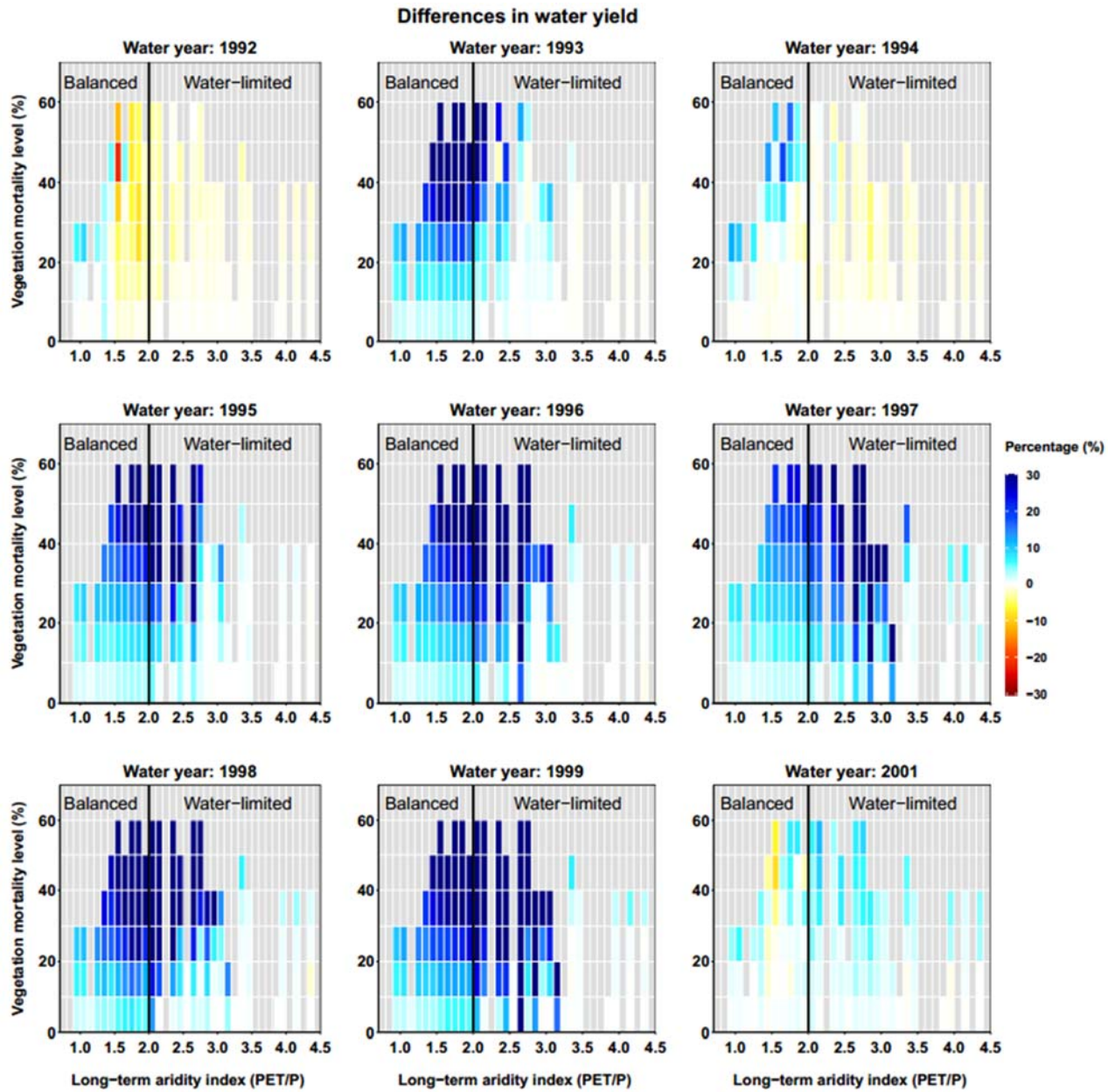
6
7



8

9 *Figure S1. The annual streamflow and precipitation for Trail Creek. The red line is the 15th*
10 *quantile of flow duration curves. Years with streamflow below the red line is water deficit years*
11 *(dry years).*

12



13

14 *Figure S2. Relationship among long-term aridity, vegetation mortality level and Differences in*
15 *water yield for 2-12 years after beetle outbreak (except for 2000).*

16

17 **1 Model parameterization**

18 1.1 Model initialization

19 We initialized soil carbon and nitrogen pools using a traditional spin up to steady state approach
20 (no changes in decadal average soil carbon and nitrogen stocks). Then we applied a target driven
21 method (Hanan et al. 2018) to initialize vegetation carbon and nitrogen stores. This method
22 allows vegetation to grow to target values based on remote sensing data, which enables us to
23 initialize mixed-age, disturbance-prone landscapes, while still providing mechanistic stability
24 and accounting for local resource limitation (e.g. local climate, nutrients, and groundwater
25 availability) (Hanan et al. 2018). For Trail Creek, we set our targets using LAI, which we
26 calculated using Landsat-5 TM reflectance data with a resolution of 30 meters. We chose the
27 clearest available growing-season scene closest to the streamflow calibration start date of 10
28 November 2010; the selected scene (Path 40, Row 30) was acquired on 02 August 2010. We
29 calculated the Normalized Difference Vegetation Index (NDVI) from TM images using Eq. (1).

$$30 \quad NDVI = \frac{\rho_{NIR^-} - \rho_R}{\rho_{NIR^+} + \rho_R} \quad (1)$$

31 In this equation, ρ_{NIR} is the reflectance in the near-infrared part of electromagnetic spectrum and
32 ρ_R is the reflectance in the red part (Hanan et al. 2018). The NDVI is used to estimate LAI by a
33 generalized NDVI-LAI model developed by Baret et al. (1989) as following Eq. (2).

$$34 \quad LAI = -\frac{1}{k} \times \ln\left(\frac{NDVI_{\infty} - NDVI}{NDVI_{\infty} - NDVI_{back}}\right) \quad (2)$$

35 Here, k represents the extinction of solar radiation through a canopy. $NDVI_{\infty}$ is the maximum
36 $NDVI$ of the region, and $NDVI_{back}$ is the background $NDVI$ (i.e., pixels without vegetation) for
37 each vegetation region. We get k value from Smith et al. (1991) for mixed pine and from White

38 et al. (2000) for other vegetation types (Hanan et al. 2018). The other parameters are calculated
 39 for each vegetation in each image (Table S1)

40 *Table S1. Normalized difference vegetation index – leaf area index (NDVI – LAI) model*
 41 *parameters for different vegetation types in Trail Creek.*
 42 *k is the extinction of solar radiation through a canopy, $NDVI_{\infty}$ is maximum NDVI observed in*
 43 *different vegetation types, and $NDVI_{back}$ is the background NDVI (not considering vegetation)*
 44 *for different vegetation types.*
 45

Vegetation	k	$NDVI_{\infty}$	$NDVI_{back}$
Pine	0.42	0.66	0.01
Deciduous	0.54	0.67	0.17
Grass	0.48	0.73	0.01
Shrub	0.55	0.71	0.06

46
 47

48 1.2 Model calibration and evaluation

49 We calibrated the coupled model against observed streamflow, which is from USGS gauge no.
 50 13137500. Six subsurface soil parameters were calibrated: saturated hydraulic conductivity
 51 (K_{sat}), the decay of K_{sat} with depth (m), pore size index (b), air-entry pressure (φ_{ac}), bypass flow
 52 to deeper groundwater storage ($gw1$), and deep groundwater drainage rates to stream ($gw2$). To
 53 account for the spatial variability of precipitation within each gridMET 4-km grid cell, we also
 54 calibrated a parameter that is used for interpolating grid-scale precipitation along elevation
 55 gradients. We selected the best parameter set by comparing observed and modeled streamflow
 56 using a multi-objective function, which includes daily Nash-Sutcliffe efficiency metric (NSE ;
 57 Nash and Sutcliffe 1970), Monthly NSE , percent error ($PerErr$) in annual flow estimates, and
 58 Pearson's Correlation Coefficient (r values larger than 0.5 are considered to be a good fit). NSE
 59 is used to compare the model fit to peak flows and it ranges from $-\infty$ to 1, where 1 means perfect

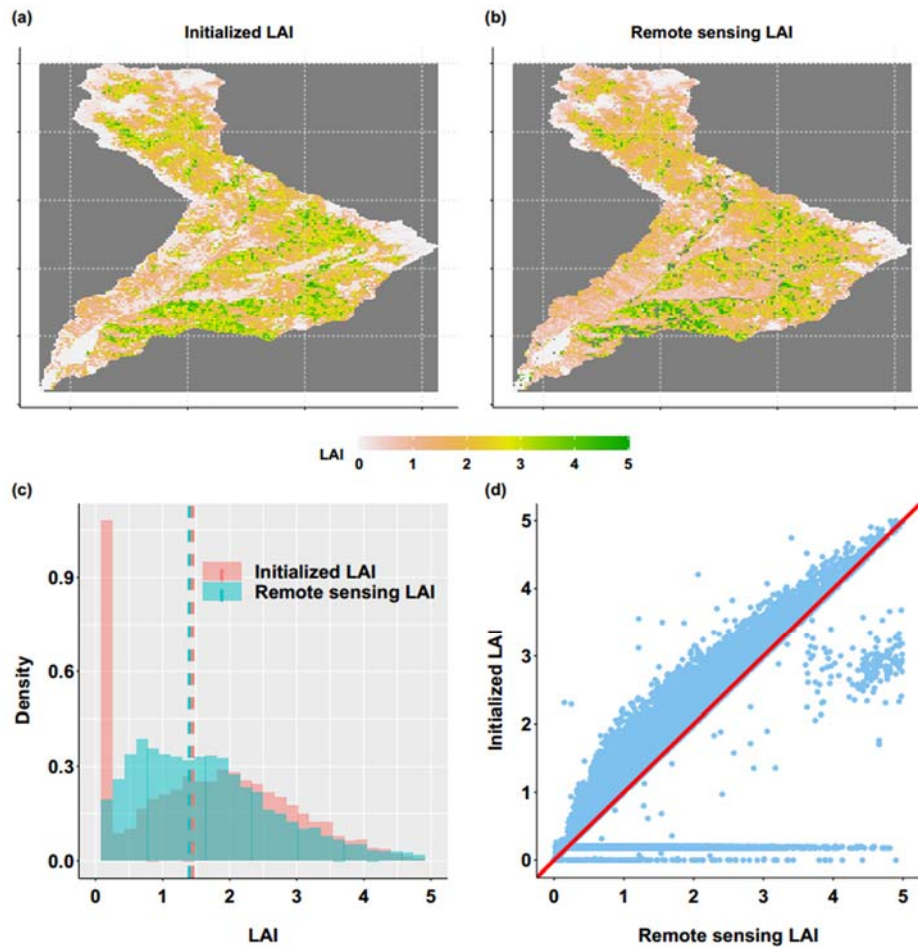
60 fit and below zero means that the mean of the observation is more accurate than the simulated
61 value. *PerErr* is used to compare differences between modeled and observed streamflow
62 volumes.

63 In addition to evaluating calibrations on streamflow, we also compared basin-scale simulated ET
64 with the Moderate Resolution Imaging Spectroradiometer (MODIS) based global data product
65 (Zhao et al. 2006; Mu et al. 2007; Zhang et al. 2009; Mu et al. 2011), and compared simulated
66 snowpack with Snow Telemetry data (SNOTEL, NRCS). These additional assessments are used
67 to determine whether good streamflow fits are for the right reasons (i.e., the important processes
68 are captured by the model). Seven years (2011 – 2017) of streamflow data, 15 years (1991-2015)
69 of SNOTEL data (Lost-Wood Divide station), and 13 years (2003 – 2015) of MODIS ET data
70 are used for this calibration and evaluation process (without special notification, we are using
71 “water year”). As to the streamflow dataset, the first five water years are used for calibration and
72 the last two years are used for evaluation.

73 **2 Model parameterization results**

74 2.1 Model initialization result

75 By using the target driving method, RHESSys successfully captured LAI heterogeneity across
76 the landscape during initialization process. As shown in Figure S3 a and b, the initialized LAI
77 matches well with remote sensing product, though some patches may slightly overshoot because
78 of the way RHESSys allocates carbon to LAI seasonally; while some other patches, mostly at the
79 top of mountains and being covered by rock or snow, are initialized with near-zero LAI but
80 remote sensing products shows some higher values. The median of simulated LAI is 3.6% higher
81 than median of remotes sensing product. Overall, the simulated LAI for model initialization is in
82 a reasonable range.



83

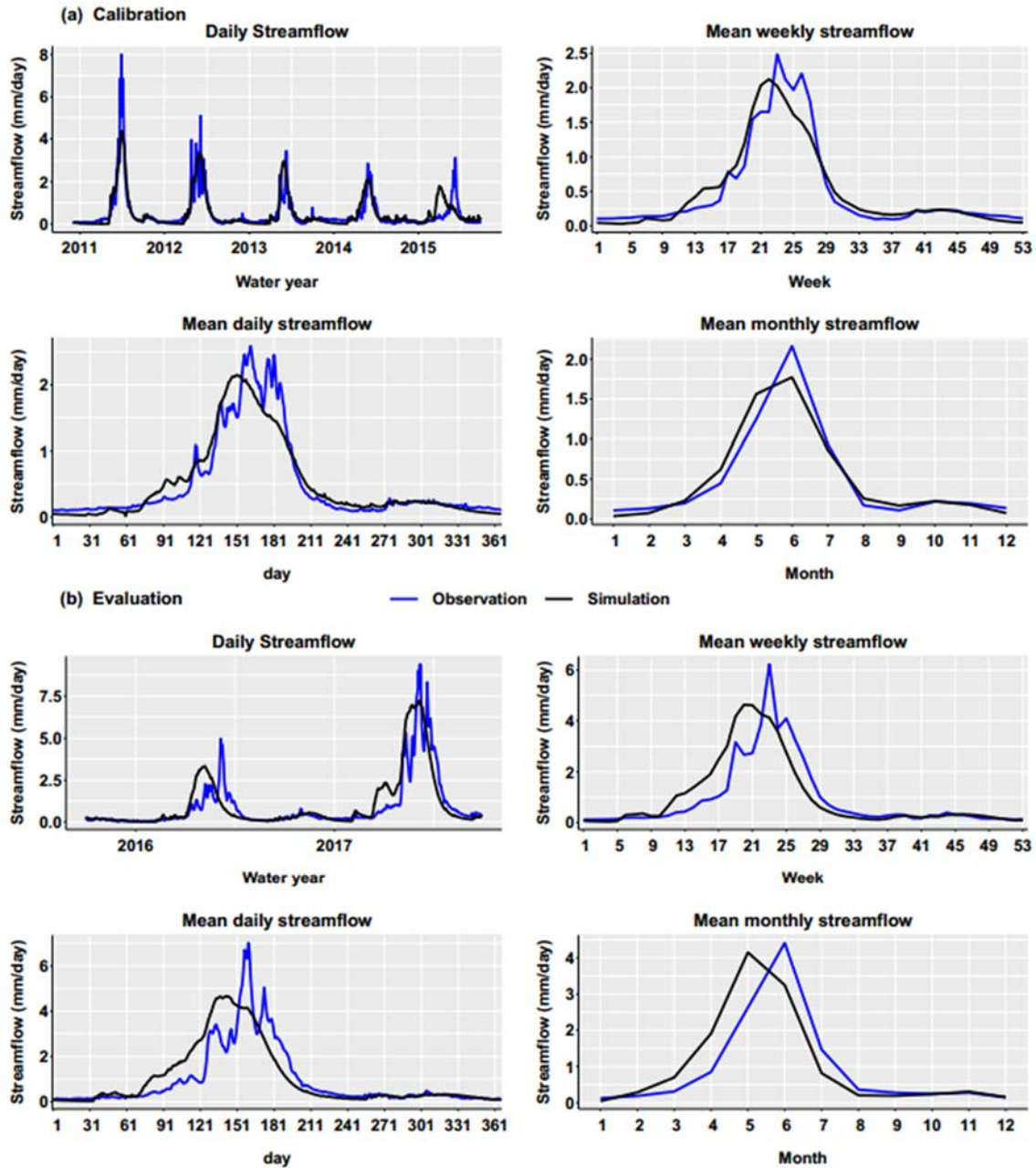
84 *Figure S3. Vegetation initialization results. We calculated LAI from a remote sensing image and*
 85 *use it as the target to initialize vegetation carbon and nitrogen for trail creek. (a) is LAI*
 86 *initialized from RHESSys model using the target-driven method (Hanan et al. 2018). (b) is the*
 87 *target LAI calculated from remote sensing data (LANDSAT 5). (c) is a comparison of the density*
 88 *distributions of LAI for the remote sensing and model initialized, dashed line is the mean of two*
 89 *LAI distributions. (d) is the scatter plot of remote sensing LAI and initialized LAI*

90

91 2.2 Model calibration and evaluation results

92 In general, the model performs satisfactorily in simulating streamflow, with slightly better
 93 performance during the calibration period than during the evaluation period (Fig. S4 and Table
 94 S2). The model can capture the seasonality of streamflow, i.e., matching peak, recession, and
 95 low flow periods. However, in some water years (e.g., 2015-2016), the timing of simulated peak
 96 flows show large bias since the model generates earlier streamflow (Fig. S4 and Table S2). This

97 is likely because RHESSys uses air temperatures to partition precipitation into rain and snow and
98 when it is near freezing, the partition errors might be large (Lundquist et al. 2008). This
99 limitation can cause poor simulation of streamflow and ET in those years, but the influence and
100 bias for modeling long-term ecohydrological fluxes are likely small (Bart et al. 2016). To further
101 test the RHESSys performance on snow accumulation, we compare the simulated snow water
102 equivalent (SWE) with SNOTEL data for the water years 1990-2015. The daily NSE is 0.93 and
103 PerError is -14%, which is in acceptable range due to this being a patch-level comparison and
104 not a basin-scale aggregation (which generally leads to higher model performance estimation).
105 We also compare simulated ET with MODIS ET for water years 2002-2017 and they show
106 similarities in annual mean and standard deviations, i.e. 725 ± 62 mm/year and $702 \pm$ mm/year
107 from the simulation and MODIS, respectively. In summary, model performance on streamflow is
108 roughly consistent for calibration and evaluation periods; the model also does a reasonably good
109 job in estimating long-term average of SWE and ET.



110

111 *Figure S4. Model calibration and evaluation in streamflow. (a) is result during calibration*
 112 *period (i.e., 2011 to 2015), and (b) is results during evaluation period (i.e., 2016-2017).*

113

114 *Table S2. Calibration and evaluation results for Trail Creek. NSE is Nash Sutcliff Efficiency and*
 115 *PerErr is total percent error, r is Pearson's correlation Coefficient. NSE is used for comparison*
 116 *of model fit of peak flows, PerErr is used to compare the differences in streamflow volumes, and*
 117 *r is used as a criterion to select better fit, which we consider r larger than 0.5 is a good fit.*

118

	Daily NSE	Monthly NSE	Percent error (%)	Pearson's correlation coefficient (r)
Calibration period (2011-2015)	0.76	0.94	2.66	0.76
Evaluation period (2016-2017)	0.71	0.73	8.62	0.74

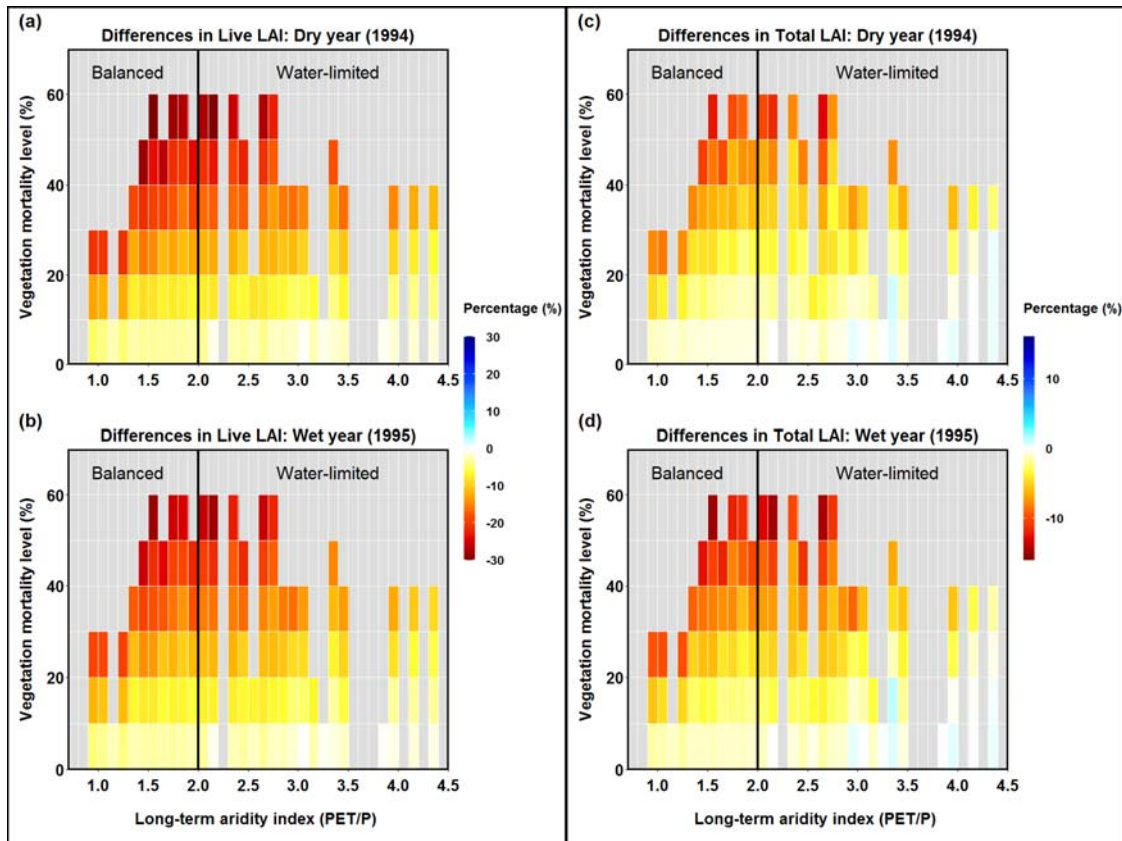
119

120 **3 Spatial result**

121 3.1 Live LAI and Total LAI

122 Figure S5 shows the relationship among long-term aridity index (x-axis), vegetation mortality
123 level (y-axis, for each sub-basin vegetation mortality is calculated as evergreen mortality
124 multiplied by evergreen coverage of that sub-basin) and changes in LAI. Live LAI decreased
125 after beetle outbreak and decreases were larger with increasing vegetation mortality (Fig. S5
126 a&b). Similarly, Total LAI decreased after beetle outbreak (and with increasing mortality) but
127 the magnitude of LAI decreases were smaller compare to Live LAI (Fig. S5 c&d). In the water-
128 limited region, Total LAI slightly increased after outbreak. The positive change in Total LAI
129 occurred because, during the years of 1994 and 1995, some portion of dead foliage was still
130 falling to the ground, while the living vegetation and understory canopy of some sub-basins grew
131 faster than before due to less competition for resources, such as water, nitrogen, and solar
132 radiation, so that Total LAI was higher than without beetle outbreak. From 1994 to 1995, some
133 portion of dead foliage continued to fall to the ground, while the residual vegetation and
134 understory continued to grow at higher rates (again, due to less competition for resources, such
135 as water, nitrogen, and radiation). If increases in growth outstripped the rate of litterfall for dead
136 foliage, there would be smaller Total LAI differences in 1994 as compared to 1995, and vice

137 versa. The Live LAI response after outbreak affects plant transpiration, and Total LAI affects
138 evaporation.



139

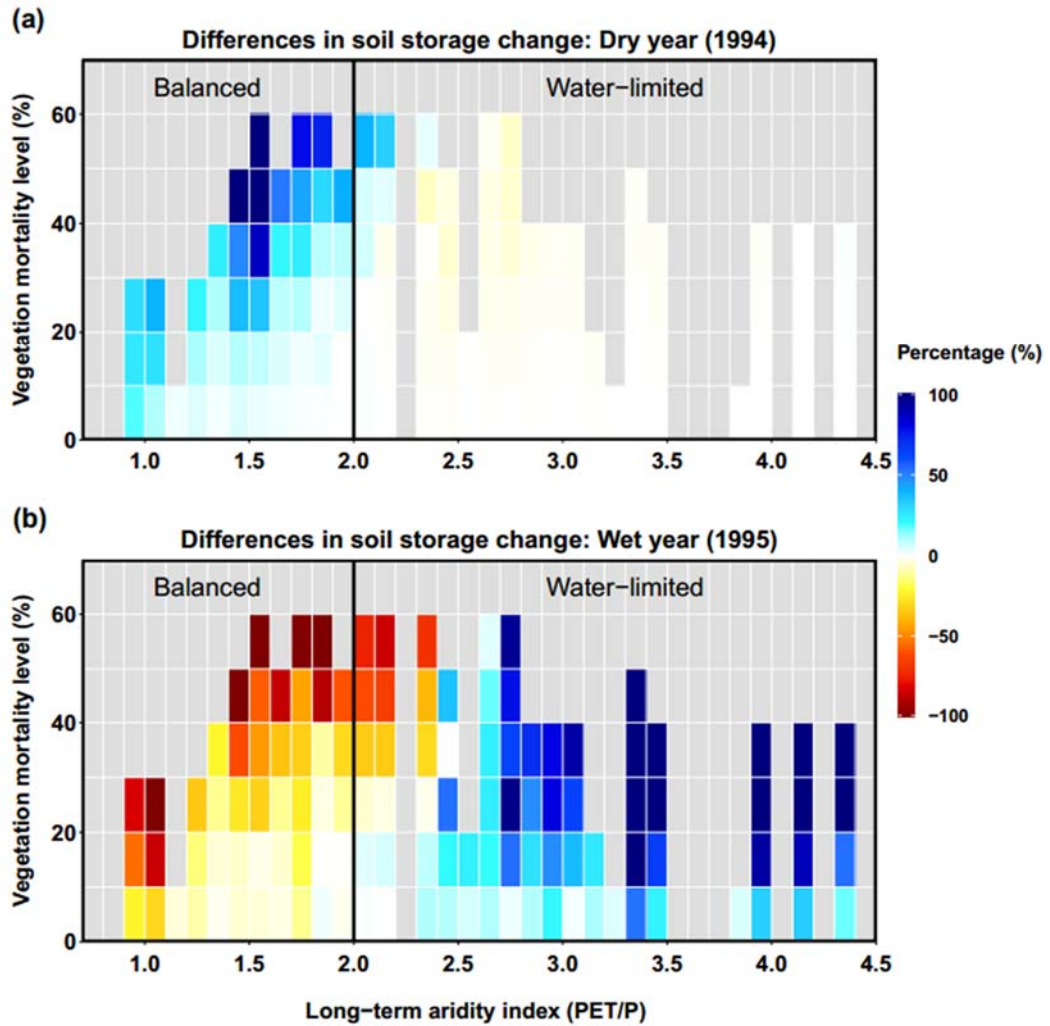
140 *Figure S5. Relationship among long-term aridity, vegetation mortality, and differences in Leaf*
141 *Area Index. Differences are calculated as the normalized differences (%) of LAI between each*
142 *evergreen mortality scenario and the control run for no beetle outbreak. Vegetation mortality for*
143 *each sub-basin is calculated as the percentage of evergreen patches multiplied by the mortality*
144 *level of evergreen caused by beetles. Long-term aridity is defined as temporally averaged (38*
145 *years) potential evapotranspiration relative to precipitation. (a) and (c) are for a dry year*
146 *(1994, 5 years after beetle outbreak), (b) and (d) are for a wet year (1995, 6 years after beetle*
147 *outbreak). (a) and (b) is Live LAI while (c) and (d) is Total LAI (i.e., LAI including dead foliage*
148 *and live leaf on the canopy).*

149

150

151 3.2 Spatial result: year-to-year soil storage change

152 The effects of beetle outbreak on year-to-year soil storage change show a conversed spatial
153 pattern during the dry year comparing with that during the wet year (Fig. S6). During a dry year,
154 the balanced area charges water in soil storage, while the water-limited area loses water from soil
155 storage. This spatial pattern matches well with effects of ET, which indicates that ET might be
156 the primary driver of the change in soil moisture during dry years (Fig. 9a & Fig. S6a). During
157 the wet year, the pattern conversed from that during the dry year: the balanced area shows
158 decreases in soil moisture, while the water-limited area shows increases (Fig. S6b). Obviously,
159 this pattern is different from that of ET (Fig. 9b & Fig. S6b). The balanced area, under high
160 precipitation condition (i.e., wet year), experiences less ET causing the soil saturated much
161 earlier than control scenario therefore, more precipitation will generate runoff. On the other
162 hand, the water-limited area, under high precipitation conditions, experiences less ET meaning
163 more precipitation will be stayed in the soil.



164

165 *Figure S6. Relationship among long-term aridity, vegetation mortality level and Differences in*
 166 *year-to-year soil storage change for a dry year (1994, a) and wet year (1995, b).*

167

168